# Gain Depletion and Recovery as a Key Mechanism of Long-Range Pulse Interactions in Soliton Fiber Laser

Dmitry A. Korobko, Valeria A. Ribenek, and Andrei A. Fotiadi

***Abstract*—Soliton interaction through gain depletion and recovery (GDR) is one of the known mechanisms of long-range pulse interactions in soliton fiber lasers. It has been commonly assumed that the GDR mechanism produces only repulsive interactions, leading to an evenly spaced pulse configuration of harmonic mode-locking. However, our theoretical investigations and numerical simulations of the GDR-induced soliton interactions in fiber lasers, mode-locked by nonlinear polarization evolution, reveal a different perspective. We have found that the GDR soliton interaction is sensitive to the generation of dispersive waves and the formation of intense soliton pedestals. These can be controlled by altering the laser polarization settings. Interestingly, under certain conditions, we observed that the GDR interaction facilitates mutual long-range attraction between solitons. Our direct numerical simulations demonstrate that depending on the polarization settings, the initial soliton configuration in the laser cavity can evolve into various multisoliton ensembles. For instance, in the final stage, a soliton group may transform into a stationary harmonic mode-locking state or evolve into a complex of bound solitons. These findings suggest a new basis for explaining the effects observed during transitions between multisoliton formations, which occur due to changes in the polarization settings of the fiber soliton laser.**

***Index Terms*—Long-range soliton interactions, mode-locking, multisoliton complexes, nonlinear polarization evolution, soliton fiber laser.**

## I. Introduction

PASSIVELY mode-locked fiber lasers, utilizing anomalous cavity dispersion, are renowned for producing ultrashort soliton pulses. These pulses are routinely generated using various mode-locking techniques, such as nonlinear polarization evolution (NPE), saturable absorber methods, and nonlinear loop mirror techniques [1], [2], [3]. A common characteristic of soliton fiber lasers is multipulse operation, where several pulses with identical energy and width are simultaneously generated in the laser cavity under strong pumping [4], [5], [6], [7]. This phenomenon is also referred to as the 'soliton energy quantization effect' [4]. These multisoliton formations display diverse dynamics, ranging from gas-like states of weakly interacting solitons to tight bunches of chaotically moving pulses, and even to soliton crystal complexes with fixed spacing between pulses [8], [9], [10], [11], [12], [13]. From an applied perspective, harmonic mode-locking (HML), where soliton pulses are evenly spaced in the laser cavity, is particularly significant [14], [15], [16]. The behavior of multisoliton ensembles in the cavity is governed by specific interactions between soliton pulses. These interactions can be categorized by their range of action. For example, direct interaction, which occurs when pulses are closely spaced, affects short-range distances of less than ten soliton durations [17]. This interaction can either trap solitons into phase-locked bound states or prevent the collapse of tight soliton bunches, inducing continuous chaotic motion within the group [9], [10], [18]. Conversely, long-range pulse interactions, acting over distances of hundreds of soliton durations, are weaker but crucial for redistributing solitons across the entire laser cavity. Various multisoliton complexes, like oscillating soliton bunches, dynamically rearranging pulse clusters, stationary loosely bound states, regular stationary structures of soliton "crystals", and HML, are formed through these long-range interactions [19], [20], [21], [22].

Soliton fiber lasers offer an excellent platform for studying nonlinear multi-particle systems, with a wide range of properties useful for applications in metrology, remote sensing, and material processing [23], [24]. The current research on long-range soliton interactions, aided by real-time ultrafast measurements [25], seeks to unveil more direct information about interaction intensities and the dynamics of processes under their influence [15], [26]. Despite intense research, the governing principles of long-range soliton interactions are only partially understood, and clarifying their physical nature remains a crucial challenge. The primary long-range interaction mechanisms include those mediated by gain depletion and recovery (GDR) processes [27], [28], [29], [30], guided acoustic wave Brillouin scattering [31], [32], [33], [34], [35], and interactions transmitted through dispersive waves (DW) or continuous wave (CW) background co-propagating with the pulses in the laser cavity (DW-interaction) [36], [37], [38]. Each mechanism has its specifics; for instance, DW-interaction, with the shortest action range (∼100 ps and less), varies in intensity based on the non-soliton component in the cavity [39]. In contrast, acoustic interaction becomes significant when the interpulse spacing is at least one nanosecond, and it aligns with the frequency of one of the fiber acoustic modes [32], [33], [34], [40]. GDR-interaction, becoming prominent with interpulse distances of several tens of picoseconds [15], is considered the most general mechanism,

Manuscript received 20 January 2024; revised 11 April 2024 and 21 May 2024; accepted 22 May 2024. This work was supported by Russian Science Foundation under Grant 23-79-30017. *(Corresponding author: Dmitry A. Korobko.)*

Dmitry A. Korobko and Valeria A. Ribenek are with Ulyanovsk State University, 432017 Ulyanovsk, Russia (e-mail: korobkotam@rambler.ru).

Andrei A. Fotiadi is with Ulyanovsk State University, 432017 Ulyanovsk, Russia, and also with the University of Mons, 7000 Mons, Belgium.

Color versions of one or more figures in this article are available at https://doi.org/10.1109/JLT.2024.3405072.

Digital Object Identifier 10.1109/JLT.2024.3405072

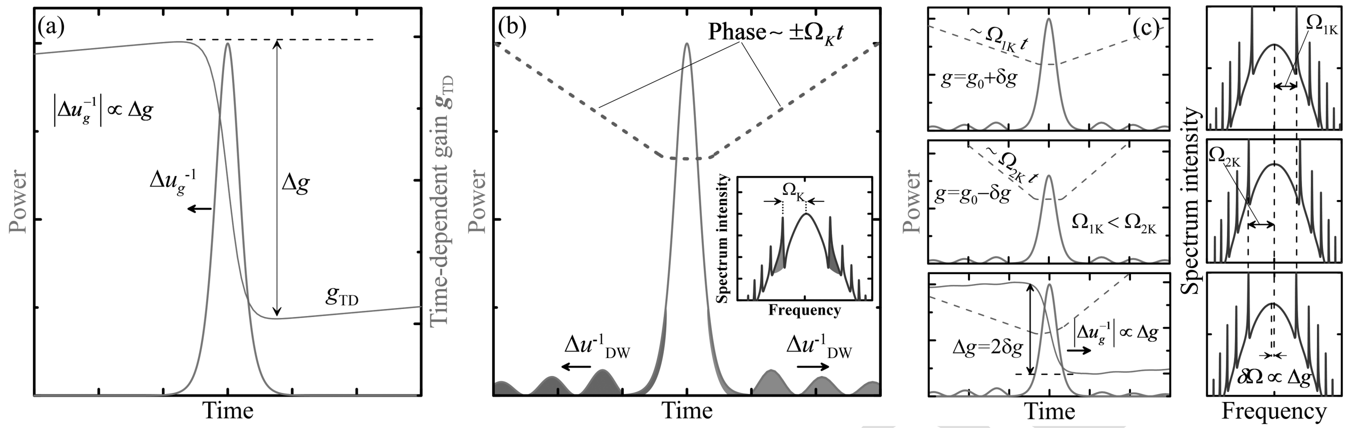


Fig. 1. Illustration to the soliton group-velocity drift due to the GDR. (a) The time-dependent depletion generates a positive group-velocity drift of the soliton toward $t \to -\infty$. (b) The soliton co-propagating with DW without the GDR effects. Directions of the DW propagations and the soliton phase dependence are also shown. Inset shows the spectrum of the soliton and co-propagating DW. $\Omega_K$ is the frequency detuning of the Kelly sideband. (c) The soliton acquiring a negative group-velocity drift due to combined action of the GDR and DW. From top to bottom: Envelope, phase dependence and spectrum of the soliton and DW when the time-independent gain is equal to $g = g_0 + \delta g$; the same but the time-independent gain is equal to $g = g_0 - \delta g$; and the same but the gain is time-dependent. It is shown that the gain asymmetry can shift the Kelly sidebands and the soliton spectrum. The 'red' shift of soliton spectrum corresponds to negative group-velocity drift to the region of lower gain towards $t \to +\infty$.

effective in fiber cavities of any length. It is traditionally believed that GDR-interaction solely leads to mutual soliton repulsion, thereby enabling HML within the fiber cavity [27]. However, existing theories fall short in explaining the universal long-range attraction necessary for generating soliton bound states or tight pulse bunches from random pulse configurations [29], leaving the explanation of transitions between various multisoliton formations as an unsolved problem.

The aim of this work is to explore the complex long-range interaction mechanism that encompasses both the GDR and DW generation. Our analysis, based on a numerical model of a fiber laser mode-locked by NPE, reveals that this complex mechanism can induce long-range soliton attraction as well as repulsion, thereby preserving the universal attributes of GDR-interaction. This mechanism's nature, whether repulsive or attractive, depends on the intensity and shape of the dispersive soliton pedestal, which is influenced by the polarization settings of the NPE mode-locking. Consequently, our model demonstrates that adjusting the polarization settings can toggle the laser between generating basic multisoliton complexes, such as chaotic bunches, HML, or bound pulse states. We propose that this model underscores the significance of the GDR as a pivotal interaction mechanism, potentially elucidating the transitions between different multisoliton formations in fiber lasers mode-locked by NPE.

## II. Soliton Group-Velocity Drift Influenced by Gain Depletion and Recovery

In our analysis, we first examine how the group velocity of a single soliton changes due to Gain Depletion and Recovery (GDR). In mode-locked lasers, the gain isn't constant over time but concentrates around each propagating pulse. Qualitatively, as a pulse traverses the gain fiber, the active ion population inversion depletes, transferring energy to the pulse. Consequently, the pulse encounters a time-dependent gain: the leading edge encounters more gain than the trailing edge. This differential results in a power flow from the trailing to the leading edge, causing the pulse to drift towards areas of higher gain ($t \to -\infty$). The magnitude of this inverse group-velocity drift correlates with the gain variation during pulse interaction $\Delta u_g^{-1} \propto \Delta g$ (Fig. 1(a)) [27]. In mode-locked fiber lasers, soliton pulses co-propagate with dispersive waves (DW) that arise from periodic disturbances due to the discrete nature of losses and amplification. The DW, forming a wide pedestal with an exponentially decaying tail, resonate with the soliton to create narrow peaks in its spectrum, known as Kelly sidebands [41], [42]. Given the anomalous cavity dispersion, high-frequency 'blue' components travel faster than 'red' ones. Thus, in the soliton frame of reference, 'blue' DW form the left wing of the pulse pedestal, moving towards $t \to -\infty$, while 'red' low-frequency components form the right wing, lagging towards $t \to +\infty$. The phase dependencies of intense dispersive components, particularly the first-order Kelly sidebands, are proportional to their frequency detunings $\propto \Omega_K$ (Fig. 1(b)). The soliton phase remains constant over time, as dispersion is completely compensated by nonlinearity. Comparing soliton and DW propagation in a fiber laser with slightly different time-independent gains (Fig. 1(c) – top two rows) we observe that the higher gain results in shorter duration and higher peak power of the soliton pulse.

The frequency detuning of the *N*-th order Kelly sideband $\Omega_{K\,N}$ relates to soliton duration $\tau_0$ as [42]:

$$\Omega_{K\,N} = (\beta_{2\Sigma})^{-1/2}\sqrt{4\pi N - \beta_{2\Sigma}/\tau_0^2}, \qquad (1)$$

where $\beta_{2\Sigma}$ is the total cavity group-velocity dispersion. Simple analysis shows that the frequency detuning $\Omega_{K\,N}$ decreases when the soliton duration $\tau_0$ decreases. Then we should conclude that the decrease of the gain $g_1 > g_2$ yields the increase of the frequency detuning $\Omega_{1K} < \Omega_{2K}$, where the $\Omega_{mK}$ is the frequency detuning of the Kelly sideband for the gain value $g_m$. In the case of the time-depending gain acting on the soliton

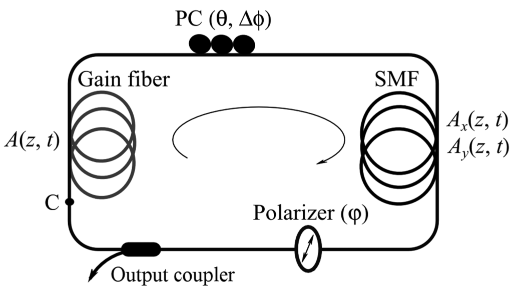


Fig. 2. The scheme of the NPE mode-locked fiber laser utilized in the numerical simulations. A detailed exposition of the model and the fixed parameter values are available in the Appendix.

one should take into account that at the leading edge of the soliton in the region of higher gain, the nonlinear effects overcompensate the dispersion. On the contrary, at the trailing edge of the pulse, the dispersion begins to dominate the nonlinearity (Fig. 1(c) – bottom row). As a result, the pulse co-propagating with DW can acquire the asymmetry of the phase dependencies of the dispersive pedestal and 'red' shift of the Kelly sidebands by the value $\delta\Omega \propto \Delta g$. Finally, the sideband asymmetry can be eliminated by the energy redistribution through nonlinear four-wave mixing (FWM) resulting in the shift of the whole soliton spectrum towards lower frequencies. In the time domain, one can see, that the DW impart a negative soliton group-velocity drift $\Delta u_g^{-1} \propto \Delta g$ to the region of lower gain towards $t \to +\infty$.

Therefore, we propose that the GDR can induce both positive and negative soliton group-velocity drifts. In order to deepen the analysis of the considered process, we endeavored to answer in detail the next questions. (i) In which cases does the joint action of the GDR and DW lead to positive, and in which to negative group-velocity drift of the soliton? (ii) Can this cooperative action induce the mechanism of pulse interaction different from the known ones mediated only by the GDR or DW? Through numerous numerical simulations of fiber laser with the GDR effects, we focus on the most common type using artificial saturable absorbers based on the NPE [43]. As we will demonstrate, varying the laser's polarization settings allows us to manipulate the soliton pedestal's shape, thereby controlling the group-velocity drift and the nature of soliton interaction.

## III. Numerical Model of NPE Mode-Locked Fiber Laser With Time-Dependent Gain

The configuration of the fiber ring laser used for numerical analysis is depicted schematically in Fig. 2. Our model of the NPE mode-locked fiber laser is similar to those referenced in [38], [44], [45], with parameter values closely mirroring those of real fiber lasers based on Er-doped gain fibers. A comprehensive description of the model is provided in the Appendix. A distinct aspect of this model is the incorporation of time-dependent gain $g_{TD}(t)$, which is a small parameter compared to the spectrally limited time-independent saturated gain $g$. This relationship is encapsulated by the inequality $g_{TD0} << g_0$, where $g_{TD0},\ g_0$ are the small signal time-dependent and time-independent gains, respectively.

Simulations reveal that when initiated with low-amplitude Gaussian noise, the laser exhibits self-starting behavior across a wide range of polarization settings, denoted as $\theta$ and $\varphi$. These settings represent the orientation angles of the polarization controller (PC) and polarizer, respectively. Within tens of cavity roundtrips facilitated by the NPE mode-locking, the laser stabilizes into sub-picosecond pulse operation, characterized by a typical soliton spectrum. Subsequent sections will delve into the dynamics of single and multiple pulse operations within the laser, specifically how they are influenced by the time-dependent gain at various polarization settings.

## IV. Simulations of the Single Soliton Drift

In this part, we will discuss the model with initial conditions as a single ultrashort soliton pulse (in considered case the gain saturation energy is constant $E_g = 75$ pJ). By investigating the soliton trajectories without the time-dependent gain $g_{TD} = 0$, we can see that they are rather different due to the fiber birefringence. Upon introducing time-dependent gain, we note that the soliton trajectory can shift either to the right or left from its original path, depending on the polarization settings $\theta$ and $\varphi$. This indicates that time-dependent gain can induce both positive and negative soliton group-velocity drifts. Fig. 3(a) shows this effect for two distinct polarization settings: 1) $\theta = 1.03,\ \varphi = 2.0$ and 2) $\theta = 0.72,\ \varphi = 2.29$. For clarity, soliton trajectories without time-dependent gain $g_{TD}$ are marked with vertical lines, illustrating the soliton shifts at specific levels of time-dependent gain for each polarization setting. Considering the simulation results for initial soliton pulse with different phases, we should conclude that the GDR-displacement of the pulse does not change with the phase variation of the initial conditions. Thus, the results shown in Fig. 3(a) confirm the hypothesis that soliton group-velocity drift is proportional to the level of time-dependent gain. The direction of this drift is influenced by the polarization settings of the NPE mode-locking, which regulate the relationship between the main soliton peak and its dispersive wings.

These relationships are illustrated by the pictures of the soliton intensity, spectrum and phase that we obtain at the input of the gain fiber for both considered polarization settings. For clearness, the evolution of the pulse and DW intensities during three cavity roundtrips is also shown (Fig. 3(b)–(g)).

One can see, that difference in cavity polarization settings leads to a change in the artificial saturable absorption and different relationships between the DW and main soliton peak. In the first case (Fig. 3(b), (d), (f)), the soliton stands out against a relatively low-intensity dispersive background, acquiring a positive group-velocity drift due to greater gain at the pulse's leading edge. In the second case (Fig. 3(c), (e), (g)), the dispersive pedestal's intensity is higher near the soliton peak but decreases rapidly toward the edges. The pulse evolution shows that the DW correct the pulse trajectory imparting a negative soliton group-velocity drift.

In the cases we considered, an optical pulse spectrum serves as a distinctive marker of the GDR and DW cooperative action on the soliton. The pulse with a negative group-velocity drift possesses a flat-topped spectrum (Fig. 3(g)), corresponding to

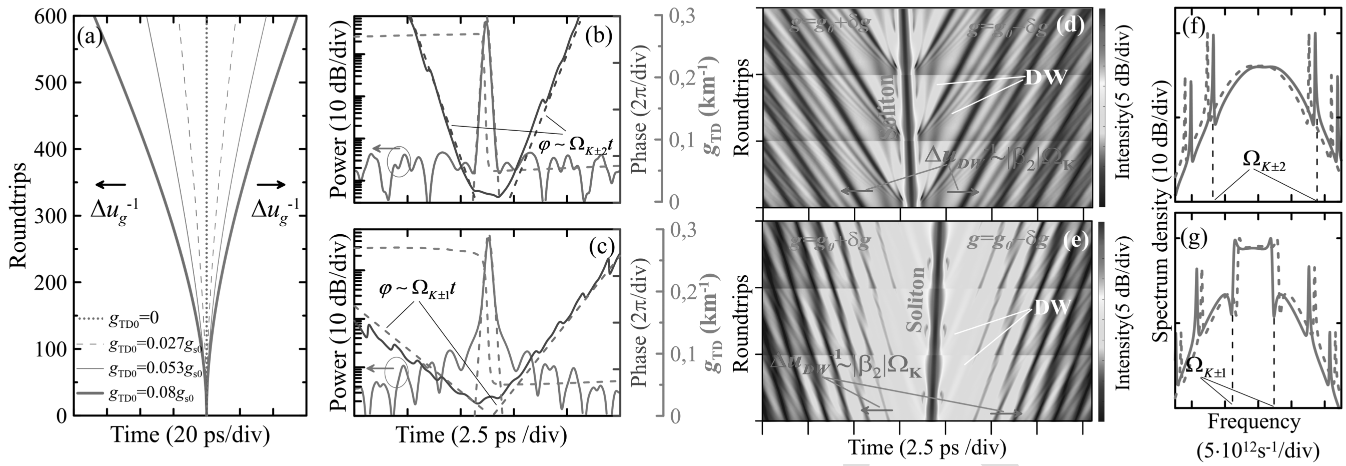


Fig. 3. Single soliton propagation caused by the GDR. (a) Soliton trajectories at different levels of the time-dependent gain. Red and blue lines are corresponding to the polarization settings $\theta = 1.03,\ \varphi = 2.0$ and $\theta = 0.72,\ \varphi = 2.29$, respectively. (b) Log-scaled intensity (red), time-dependent gain (magenta dashed) and phase dependence (green) of the pulse propagating in the steady state of the fiber laser with the polarization settings $\theta = 1.03,\ \varphi = 2.0$ and $g_{TD0} = 0.08 g_{s0}$. Red-dashed line shows the intensity of the initial soliton, green dashed lines fit the DW phase by the linear dependencies proportional to the frequency detuning of the most powerful Kelly sidebands $\Omega_{K\pm N}$. All the curves are built for the point C corresponding to the gain fiber input. (c) The same as (b), but for the polarization settings $\theta = 0.72,\ \varphi = 2.29$; log-scaled soliton intensity are shown by the blue line. (d) Evolution of the pulse and DW during three cavity roundtrips with polarization setting corresponding to Fig. 3(b). (e) The same as (d), but for polarization settings corresponding to Fig. 3(c). (f) Spectrum corresponding to the pulse shown in Fig. 3(b). (g) Spectrum corresponding to the pulse shown in Fig. 3(c). The dashed lines show the spectra without the time-dependent gain.

a soliton with powerful first-order Kelly sidebands located at small frequency detunings $\Omega_{K\pm1}$. Gain asymmetry provides 'red' shift of the Kelly sidebands and slight change of the DW velocities $\Delta u_{DW}^{-1}$. Under conditions specified above, the ratio of DW energy to the energy of the soliton is close to the maximum and the phase dependencies of the soliton and dispersive background merge seamlessly (Fig. 3(c)) resulting in efficient FWM process that corrects the soliton trajectory to the region of lower gain.

Conversely, the energy of the soliton in Fig. 3(b) is significantly higher. A higher peak power leads to an increase in the phase difference between the soliton and DW and the disappearance of the first-order Kelly sidebands. (The expression under the square root in (1) becomes negative at $N = 1$). Thus, in fact, the most intensive Kelly sidebands shown in the inset of Fig. 3(d) are of the next (second) order with the greater frequency detunings $\Omega_{K\pm2}$. The DW energy decreases and the phase of the dispersive background sharply contrasts with the soliton phase, so the efficiency of the FWM between the DW and soliton is negligible and the dynamics of the 'Soliton+DW' system in this case is entirely determined by the soliton acquiring a positive group-velocity drift to the region of higher gain.

Additionally, we in detail show the evolution of the intensity and spectrum of the soliton and DW in each of the characteristic cases (positive or negative group-velocity drift) in Supplementary materials, where we use a known methodology of decomposing the simulated ultrashort pulse into a fundamental soliton and DW [46]. These materials demonstrate the specific features and relationships between the intensity and the spectrum of the soliton and DW as they pass through the laser cavity (similarly Fig. 3(d), (e)). In particular, we draw attention to the significant change in the pulse spectrum and profile of the dispersion pedestal during this evolution.

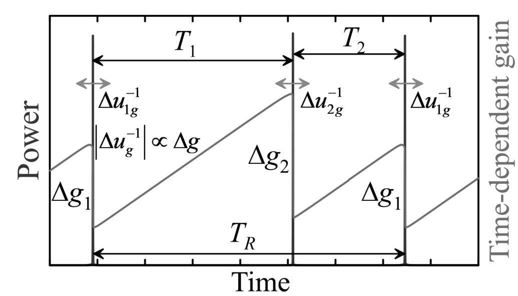


Fig. 4. The scheme of the GDR interaction of two pulses in the cavity with fundamental period $T_R$.

## V. Soliton Interaction Through Gain Depletion and Recovery

A key insight from the preceding sections is that pulses in a fiber laser mode-locked by the NPE can interact through the GDR mechanism, exhibiting either repulsion or attraction based on the polarization settings. This concept is illustrated in Fig. 4, which depicts the GDR interaction of two pulses within a fiber cavity having a fundamental period $T_R$. This interaction can be likened to that of two compact objects separated by time distances $T_1, T_2$ ($T_1 + T_2 = T_R$). Under the influence of one of the pulses, the velocity of another pulse gets incremental change by the value $\Delta u_{ig}^{-1}$ and vice versa, so the relative pulse velocity changes by $(\Delta u_{1g}^{-1} - \Delta u_{2g}^{-1})$. Also, it means that the centers of mass of the spectra of each of the pulses are slightly shifted from each other. The strength of the pulse interaction depends on the time distances $T_1$ and $T_2$. Results obtained above show that the value of the group-velocity drift is proportional to the gain depletion $\Delta u_{ig}^{-1} = a\, \Delta g_i$. From simple analysis, we can find that if initially the time distances relate as $T_1 > T_2$, then the next inequality is true for the local gain values: $g_2 > g_1$ since the gain has more time to recover before the second pulse. Thus, it leads to the inequality $\Delta g_2 > \Delta g_1$, and as a result $|\Delta u_{2g}^{-1}| > |\Delta u_{1g}^{-1}|$ (Fig. 4). Fig. 4 presents the scheme of the GDR interaction between two pulses in a cavity with a fundamental period $T_R$. When the group-velocity drifts are directed leftwards (towards $t \to -\infty$), the faster second pulse moves away from the first, a phenomenon known as the GDR pulse repulsion occurs. This leads to the equalization of inter-pulse distances and harmonic mode-locking [27]. Conversely, if the velocity drifts are directed rightwards (towards $t \to +\infty$), the slower first pulse is 'caught up' by the faster second pulse, resulting in pulse attraction. Our findings demonstrate that the GDR-induced group-velocity drifts can be manipulated by modifying the polarization settings of the NPE mode-locked fiber laser. By adjusting polarization angles $\theta$ and $\varphi$ one can control the forces of soliton interaction, such as converting soliton repulsion into attraction. This newfound aspect of the GDR soliton interaction provides an explanation for the transitions between multisoliton complexes that occur when the polarization settings of the NPE mode-locked fiber laser are altered.

We consider a pair of examples of forming various soliton ensembles influenced by the GDR effects in our numerical model. The first example relates to soliton repulsion, defined by polarization settings that lead to positive group-velocity drift $\theta = 1.03,\ \varphi = 2.0$. Here, the initial conditions involve four solitons with non-periodic positions in the cavity, with initial inter-pulse time distances of $T_1 = 205.36$ ps, $T_2 = T_3 = T_4 = 150$ ps. The final results do not depend on phase relation between the initial pulses. Fig. 5(a) shows the evolution of the soliton arrangement in the fiber cavity under the GDR-induced soliton repulsion. During this evolution and after tens of thousands of cavity roundtrips, the repelling pulses eventually distribute evenly throughout the cavity (Fig. 5(b)), i.e., the jumps in gain depletion $\Delta g_i$ are equalized, inducing the alignment of drift velocities and the shift of the spectrum of each of the individual pulses towards a common center of mass (Fig. 5(d)). As one can see, the spectrum shape is close to the spectrum of single soliton with positive $\Delta u_g^{-1}$.

We should also emphasize that the scales of the GDR-interaction that we study are not limited to hundreds of ps and we are exploring global long-range interactions on the scale of the entire cavity (up to hundreds of ns and more). The fact that inter-pulse distances of up to hundreds of ps are considered in the presented numerical modeling is only due to the restricted capabilities of simulator, but even at these limited scales, the GDR mechanism can dominate over direct DW interaction. Thus, we have additionally performed a series of numerical simulations of the interaction of several pulses, in which, for comparison, the effect of time-dependent gain was completely "turned off" (Fig. 5(c)). Slightly oscillating pulse trajectories demonstrate that under considered conditions the intensity of the direct DW interaction mechanism is negligible comparing to the GDR-interaction.

Subsequent example focuses on soliton attraction scenario (Fig. 6). Fig. 6(a) shows the intracavity dynamics of two solitons under polarization settings $\theta = 0.9,\ \varphi = 2.53$, which induce negative group-velocity drift due to the cooperative action of the GDR and DW. Initially, the solitons are subject to an attractive force, drawing them closer. After about thousands of cavity roundtrips, the distance between the solitons decreases, and as the pulses gradually approach each other, the attractive

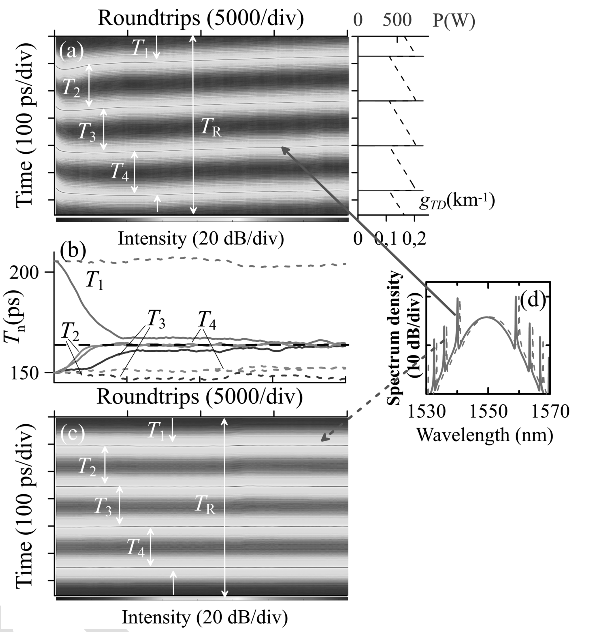


Fig. 5. Numerical simulation of the harmonic mode-locking of four repelling pulses. Polarization settings are$\theta = 1.03,\ \varphi = 2.0$. (a) Field evolution within the cavity (left); the arrangement of the solitons (blue solid lines) and the time-dependent gain (dashed lines) after 20 000 cavity roundtrips (right). For convenience, the pulses evolution is shown in a moving coordinate frame. (b) Changes of the inter-pulse time distances. The black dashed line shows the inter-pulse time distance corresponding to the HML state. The colored dashed lines show the changes of the inter-pulse time distances when the time-dependent gain is "turned off". (c) Field evolution within the cavity when the time-dependent gain is "turned off". (d) The spectrum of the single pulse corresponding to the HML state. The dashed line shows the spectrum of the single pulse in Fig. 5(c).

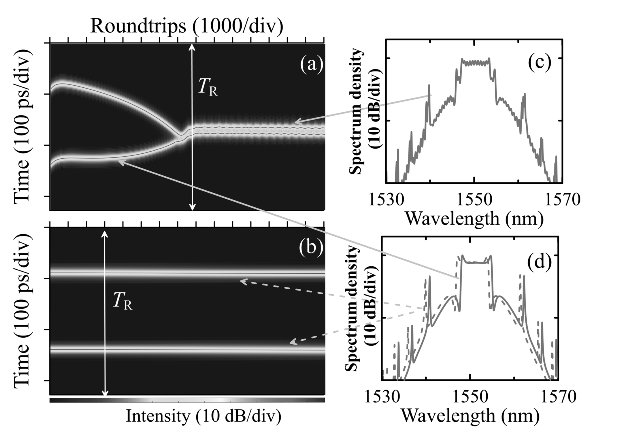


Fig. 6. (a) Numerical simulation of attraction of two solitons. Field evolution within the cavity. The polarization settings are $\theta = 0.9,\ \varphi = 2.53$. (b) Field evolution within the cavity with the same polarization settings, but the time-dependent gain is "turned off". (c) The spectrum of the bound soliton state in the final of evolution in Fig. 6(a). (d) The spectrum of the single attracting pulse in Fig. 6(a). The dashed line shows the spectrum of the single pulse in Fig. 6(b).

forces and the repelling forces induced by the direct DW-interaction eventually balance out. This results in two solitons co-propagating with a slightly oscillating inter-pulse time distance, approximately equating to tens of soliton durations, thereby forming a loosely bound soliton state. The change of the phase difference between initial pulses leads only to some variation of the oscillation period and inter-pulse distance in final bound soliton state without affecting the mutual pulse attraction at the first stage. The spectrum shape of the single pulse in the stage of attraction (Fig. 6(d)) is close to the spectrum of single soliton with negative group-velocity drift. Ultimately, after formation of the bound state, the drift velocities become almost equal and the pulses form the joint spectrum with interference fringes typical for a bound state of the solitons (Fig. 6(c)).

For comparison, the Fig. 6(b) demonstrates the evolution of two pulses when the effect of time-dependent gain is completely “turned off”. In this case, the pulses can interact only through the direct DW-interaction. Despite the fact that the spectrum of interacting pulses differs from that shown in Fig. 5(d) (compare with Fig. 6(d)), one can see that the intensity of direct DW-interaction is still insufficient for the mutual pulse attraction or repulsion, emphasizing the fundamental importance of considering effect of time-dependent gain.

## VI. Discussion and Conclusion

In this study, we have examined the long-range soliton interactions in a soliton fiber laser mode-locked by nonlinear polarization evolution (NPE), with a particular focus on the interactions induced by the Gain Depletion and Recovery (GDR) mechanism. A unique aspect of our approach is the consideration of effects related to the generation of resonant dispersive waves, which form soliton pedestals and can be manipulated via polarization settings. Our findings indicate that the generation of dispersive waves (DW) significantly influences the GDR soliton interaction process. Conventionally, it has been believed that the GDR mechanism imparts a positive group-velocity drift to propagating pulses, leading to a harmonic mode-locking state in the laser [27]. However, our research suggests that under certain conditions, the combined effect of the GDR mechanism and DW generation can induce a negative group velocity drift in solitons, significantly altering the collective dynamics of solitons within the cavity. These conditions involve the formation of an intense, inhomogeneous soliton pedestal that influences the soliton phase. Crucially, the shape of this soliton pedestal can be modulated by adjusting the polarization settings of the NPE mode-locked laser. We believe that the shape of pulse spectrum can serve as a distinctive marker of the result of cooperative GDR+DW action on the pulse. The soliton spectrum with pronounced Kelly sidebands with large frequency detunings $\Omega_K$ is typical for the case of substantial group velocity difference between the soliton and DW: $\Delta u_{DW}^{-1} \approx |\beta_2|\Omega_K$. At this point, the soliton energy significantly exceeds the energy of the DW and dynamics of the system is entirely determined by the soliton acquiring a positive group-velocity drift under the action of the GDR. Conversely, flat-topped spectrum corresponding to a soliton with Kelly sidebands located at small frequency detunings $\Omega_K$ is a sign of possible negative group velocity drift, which can be induced by the GDR through ‘red’ shift of the Kelly sidebands and efficient FWM process.

Through direct numerical simulations of soliton interactions within the fiber cavity, we have discovered that the GDR mechanism can facilitate not only soliton repulsion (in case of positive group velocity drift) but also a previously unexplored phenomenon of the GDR-induced soliton attraction, which corresponds to negative group velocity drift of interacting pulses. We also note that the shape of the optical spectrum continues to be an indicator of the interaction type. Flat-topped spectrum is a characteristic of attracting pulses, while repelling pulses have typical soliton spectrum with pronounced Kelly sidebands. A qualitative confirmation of our results is that a number of fiber laser experimental works report on the generation of a bunch of mutually attracted solitons possessing flat-topped spectrum with closely spaced Kelly sidebands. [47], [48], [49], [50], [51].

It is also important to note the specific features of considered mechanism that fundamentally distinguish it from direct DW-interaction. Firstly, the mechanism mediated by the cooperative action of GDR and DW acts on the scale of the entire cavity. Its range is limited only by the relaxation time of ion population $\sim 10^{-3}$ s. Secondly, the nature of the mechanism implies the interaction between the soliton and DW generated by the same soliton, i.e., the result of the multisoliton interaction is independent on phase difference between the interacting pulses.

Our simulations further reveal that, in a fiber laser model with GDR interaction, the initial soliton group can evolve into various types of multisoliton ensembles, depending on the polarization settings. These ensembles can be a stationary harmonic mode-locking (HML) state, or form complex bound solitons. We propose that the full spectrum of multisoliton dynamics can be uncovered by exploring a wide range of intermediate polarization settings. These settings regulate the intensity of interacting forces among solitons in the model of the soliton fiber laser with the GDR interaction. Therefore, our results lay a foundation for understanding the effects and transitions between different multisoliton formations that occur due to changes in polarization settings. This understanding enhances our knowledge of the processes occurring in the cavity of the NPE mode-locked fiber soliton lasers.

## Appendix
## Numerical Model of the NPE Mode-Locked Fiber Laser With Time-Dependent Gain

The numerical simulations employ a configuration of a fiber ring laser, which includes a gain medium, a polarization controller (PC), a segment of passive single-mode fiber (SMF), a polarizer, and an output coupler. We assume linear polarization of light in the gain fiber, while the light in the SMF can have elliptical polarization. The optical field amplitude's evolution in the gain fiber of length $l_a$ is governed by the generalized NLS equation:

$$\frac{\partial A}{\partial z} - i\frac{\beta_{2g}}{2}\frac{\partial^2 A}{\partial t^2} - i\gamma_g|A|^2A = \frac{gA}{2} + \frac{g}{2\Omega_g^2}\frac{\partial^2 A}{\partial t^2}, \qquad (1A)$$

where, $A$ is the complex amplitude of the linearly polarized electric field in the gain fiber, $z$ is the coordinate along the fiber, $\beta_{2g}$ is the group velocity dispersion (GVD) of the fiber, and $\gamma_g$ is the Kerr nonlinearity of the gain fiber. The gain spectral filtering is centered at the wavelength $\lambda_0$ and employed in parabolic approximation with the FWHM gain line bandwidth $\Omega_g$. The saturated time-independent gain $g$ is averaged over the simulation window and is expressed as

$$g(z,t) = g(z) = g_0 \exp\left(-\frac{1}{E_g}\int_0^{\tau_{win}} |A(z,t)|^2 dt\right) \quad (2A)$$

where $g_0$ is a small signal gain and $E_g$ is the gain saturation energy determined by the pump power, $\tau_{win}$ is the width of the simulation window. At the output of the gain fiber, the polarization state of light inside the passive fiber (SMF) is set by the polarization controller (PC) as$A_x = A\cos\theta,\ A_y = A\sin\theta\exp\Delta\phi$, where $\theta$ is the angle between the polarization direction of the input light and the fast axis of the SMF, which can be tuned by adjusting the PC, $\Delta\phi$ is the birefringence of the PC.

The light propagation in the birefringent passive single-mode fiber (SMF) of length $l_{SMF}$ is described by the two coupled nonlinear Schrodinger equations:

$$\begin{aligned}&\frac{\partial A_X}{\partial z} - i\frac{\Delta\beta}{2}A_X + \delta\frac{\partial A_X}{\partial t} - i\frac{\beta_2}{2}\frac{\partial^2 A_X}{\partial t^2}\\&- i\gamma\left(|A_X|^2 + \frac{2}{3}|A_Y|^2\right)A_X - \frac{i}{3}\gamma A_X^* A_Y^2 = 0,\\&\frac{\partial A_Y}{\partial z} + i\frac{\Delta\beta}{2}A_Y - \delta\frac{\partial A_Y}{\partial t} - i\frac{\beta_2}{2}\frac{\partial^2 A_Y}{\partial t^2}\\&- i\gamma\left(|A_Y|^2 + \frac{2}{3}|A_X|^2\right)A_Y - \frac{i}{3}\gamma A_Y^* A_X^2 = 0, \quad (3A)\end{aligned}$$

where $A_X$ and $A_Y$ are the field amplitudes of two polarization components, $\Delta\beta = 2\pi/L_B$ – birefringence of the SMF, $\delta = \Delta\beta/\omega_0, \omega_0 = 2\pi c/\lambda_0$. The effects of cross-modulation and four-wave mixing are taken into account by the third and fourth terms in (3A). To avoid the effects associated with the fiber cavity inhomogeneity, the gain fiber and the SMF are assumed to have the same nonlinearity $\gamma_g = \gamma$ and GVD $\beta_{2g} = \beta_2$. Finally, the polarizer returns the state of linear polarization $A = A_x\cos\varphi\ + A_y\sin\varphi$, where $\varphi$ is the polarizer orientation angle. The block combining the PC, birefringent SMF and the polarizer operates as a saturable absorber. Its transmission involving NPE is a function of the input signal power $|A|^2$ that at a certain set of parameters ensures the laser mode-locking, providing the generation of an ultrashort pulse [43]. All the linear losses experienced by the signal within the cavity are taken into account as the local losses in the output coupler described by its power transmission coefficient $\rho^2$: $A' = \rho A$.

The key feature of the numerical model is consideration of the GDR effects introduced by the time-dependent gain factor $g_{TD}(t)$, which is determined by the standard rate equation

$$\frac{dg_{TD}}{dt} = \frac{g_{TD0} - g_{TD}}{\tau_g} - \frac{g_{TD}|A(z,t)|^2}{E_g}, \quad (4A)$$

TABLE I
THE SYSTEM PARAMETERS USED IN SIMULATIONS

| Parameter | Value | Parameter | Value |
|---|---|---|---|
| $\lambda_0$ (nm) | 1550 | $\Omega_g/2\pi$ (THz) | 10.5 (~ 85 nm in the range near $\lambda_0 = 1550$ nm) |
| $\gamma$ (W$^{-1}$ m$^{-1}$) | 0.002 | $g_0$ (m$^{-1}$) | 1.5 |
| $\beta_2$ (ps$^2$m$^{-1}$) | -0.02 | $E_g$ (pJ) | $k\cdot 75$ (k is the number of pulses) |
| $\rho$ | 0.85 | $l_{SMF}$ (m) | 8 |
| $\Delta\varphi$ | $\pi/12$ | $l_a$ (m) | 2 |
| $L_B$ (m) | 3.64 | $\tau_g$ ($\mu s$) | 0.5 |

where $\tau_g$ – is the relaxation time of the gain medium; $g_{TD0} <<$ $g_0$– is the initial level of unsaturated time-dependent gain. Comparing the system with and without time-dependent gain $g_{TD}(t)$ we should correct the spectrally limited gain value $g$ as$g' = g - g_m/2$, where $g_m$ – is the maximum value of the time-dependent gain $g_{TD}(t)$; $g'$, $g$ are the spectrally limited gain factors for the system with and without the time-dependent gain, respectively.

The most of cavity parameters used for calculations are typical for the real fiber laser of telecom range on the base of Er-doped gain fiber and listed in Table I.

Periodic boundary conditions with window size $\tau_{win} = 2^{14}\cdot 0.01$ ps $\cdot\, k$ ($k$ is the number of simulated pulses in the cavity) consisting of $2^{14}\cdot k$ points are used for simulation. In this instance the value of $\tau_{win}$ corresponds to the fundamental period of the cavity $T_R$. Note that for real lasers, the values of the parameters $\tau_g$ and $T_R$ exceed the selected ones by a factor of thousands. It has been done to speed up the simulation. Nevertheless, the choice fully satisfies the necessary condition $T_R << \tau_g$ and is adequate to describe the soliton interaction through the GDR.

## REFERENCES

[1] W. Fu, L. G. Wright, P. Sidorenko, S. Backus, and F. W. Wise, "Several new directions for ultrafast fiber lasers," *Opt. Exp.*, vol. 26, no. 8, pp. 9432–9463, Apr. 2018, doi: 10.1364/OE.26.009432.
[2] L. Dai et al., "Carbon nanotube mode-locked fiber lasers: Recent progress and perspectives," *Nanophotonics*, vol. 10, no. 2, pp. 749–775, Nov. 2020, doi: 10.1515/nanoph-2020-0446.
[3] I. T. Sorokina, V. V. Dvoyrin, N. Tolstik, and E. Sorokin, "Mid-IR ultrashort pulsed fiber-based lasers," *IEEE J. Sel. Topics Quantum Elect.*, vol. 20, no. 5, pp. 99–110, Sep./Oct. 2014, doi: 10.1109/JSTQE.2014.2310655.
[4] D. Y. Tang, L. M. Zhao, B. Zhao, and A. Q. Liu, "Mechanism of multisoliton formation and soliton energy quantization in passively mode-locked fiber lasers," *Phys. Rev. A*, vol. 72, no. 4, Oct. 2005, Art. no. 043816, doi: 10.1103/PhysRevA.72.043816.
[5] X. Liu, "Hysteresis phenomena and multipulse formation of a dissipative system in a passively mode-locked fiber laser," *Phys. Rev. A*, vol. 81, no. 2, Feb. 2010, Art. no. 023811, doi: 10.1103/PhysRevA.81.023811.
[6] Y. Jeong, L. A. Vazquez-Zuniga, S. Lee, and Y. Kwon, "On the formation of noise-like pulses in fiber ring cavity configurations," *Opt. Fiber Technol.*, vol. 20, no. 6, pp. 575–592, Dec. 2014, doi: 10.1016/j.yofte.2014.07.004.
[7] D. A. Korobko, V. A. Ribenek, P. A. Itrin, and A. A. Fotiadi, "Birth and annihilation of solitons in harmonically mode-locked fiber laser cavity through continuous wave injection," *Opt. Fiber Technol.*, vol. 75, Jan. 2023, Art. no. 103216, doi: 10.1016/j.yofte.2022.103216.
[8] F. Amrani, A. Haboucha, M. Salhi, H. Leblond, A. Komarov, and F. Sanchez, "Dissipative solitons compounds in a fiber laser. Analogy with the states of the matter," *Appl. Phys. B*, vol. 99, no. 1/2, pp. 107–114, Oct. 2009, doi: 10.1007/s00340-009-3774-7.

[9] D. A. Korobko, R. Gumenyuk, I. O. Zolotovskii, and O. G. Okhotnikov, “Multisoliton complexes in fiber lasers,” *Opt. Fiber Technol.*, vol. 20, no. 6, pp. 593–609, Dec. 2014, doi: 10.1016/j.yofte.2014.08.011.

[10] L. M. Zhao, D. Y. Tang, H. Zhang, and X. Wu, “Bunch of restless vector solitons in a fiber laser with SESAM,” *Opt. Exp.*, vol. 17, no. 10, pp. 8103–8108, Apr. 2009, doi: 10.1364/oe.17.008103.

[11] J. Rissanen, D. A. Korobko, I. O. Zolotovsky, M. Melkumov, V. F. Khopin, and R. Gumenyuk, “Infiltrated bunch of solitons in bi-doped frequency-shifted feedback fibre laser operated at 1450 nm,” *Sci. Rep.*, vol. 7, no. 1, Mar. 2017, Art. no. 44194, doi: 10.1038/srep44194.

[12] A. Haboucha, H. Leblond, M. Salhi, A. Komarov, and F. Sanchez, “Analysis of soliton pattern formation in passively mode-locked fiber lasers,” *Phys. Rev. A*, vol. 78, no. 4, Oct. 2008, Art. no. 043806, doi: 10.1103/physreva.78.043806.

[13] A. Kokhanovskiy et al., “Multistability manipulation by reinforcement learning algorithm inside mode-locked fiber laser,” *Nanophotonics*, Apr. 2024, doi: 10.1515/nanoph-2023-0792.

[14] C. Lecaplain and P. Grelu, “Multi-gigahertz repetition-rate-selectable passive harmonic mode locking of a fiber laser,” *Opt. Exp.*, vol. 21, no. 9, pp. 10897–10902, Apr. 2013, doi: 10.1364/oe.21.010897.

[15] X. Liu and M. Pang, “Revealing the buildup dynamics of harmonic mode-locking states in ultrafast lasers,” *Laser Photon. Rev.*, vol. 13, no. 9, Aug. 2019, Art. no. 1800333, doi: 10.1002/lpor.201800333.

[16] D. Korobko et al., “Stabilization of a harmonic mode-locking by shifting the carrier frequency,” *J. Lightw. Technol.*, vol. 39, no. 9, pp. 2980–2987, May 2021, doi: 10.1109/jlt.2021.3068822.

[17] V. V. Afanasjev and N. Akhmediev, “Soliton interaction in nonequilibrium dynamical systems,” *Phys. Rev. E*, vol. 53, no. 6, pp. 6471–6475, Jun. 1996, doi: 10.1103/physreve.53.6471.

[18] R. Weill, A. Bekker, V. Smulakovsky, B. Fischer, and O. Gat, “Spectral sidebands and multipulse formation in passively mode-locked lasers,” *Phys. Rev. A*, vol. 83, no. 4, Apr. 2011, Art. no. 043831, doi: 10.1103/physreva.83.043831.

[19] S. Chouli and P. Grelu, “Soliton rains in a fiber laser: An experimental study,” *Phys. Rev. A*, vol. 81, no. 6, Jun. 2010, Art. no. 063829, doi: 10.1103/physreva.81.063829.

[20] T. Zhu, Z. Wang, D. N. Wang, F. Yang, and L. Li, “Observation of controllable tightly and loosely bound solitons with an all-fiber saturable absorber,” *Photon. Res.*, vol. 7, no. 1, pp. 61–68, Dec. 2018, doi: 10.1364/prj.7.000061.

[21] A. V. Andrianov, “All-optical manipulation of elastic soliton crystals in a mode-locked fiber laser,” *IEEE Photon. Technol. Lett.*, vol. 34, no. 1, pp. 39–42, Jan. 2022, doi: 10.1109/lpt.2021.3135585.

[22] V. A. Ribenek, D. A. Stoliarov, D. A. Korobko, and A. A. Fotiadi, “Mitigation of the supermode noise in a harmonically mode-locked ring fiber laser using optical injection,” *Opt. Lett.*, vol. 46, no. 22, pp. 5747–5750, Nov. 2021, doi: 10.1364/ol.441630.

[23] D. Chaparro and S. Balle, “Optical addressing of pulses in a semiconductor-based figure-of-eight fiber laser,” *Phys. Rev. Lett.*, vol. 120, no. 6, Feb. 2018, Art. no. 064101, doi: 10.1103/physrevlett.120.064101.

[24] J. K. Jang, M. Erkintalo, S. Coen, and S. G. Murdoch, “Temporal tweezing of light through the trapping and manipulation of temporal cavity solitons,” *Nature Commun.*, vol. 6, no. 1, Jun. 2015, Art. no. 7370, doi: 10.1038/ncomms8370.

[25] A. Mahjoubfar, D. V. Churkin, S. Barland, N. Broderick, S. K. Turitsyn, and B. Jalali, “Time stretch and its applications,” *Nature Photon.*, vol. 11, no. 6, pp. 341–351, Jun. 2017, doi: 10.1038/nphoton.2017.76.

[26] J. Zeng and M. Y. Sander, “Real-time transition dynamics between multi-pulsing states in a mode-locked fiber laser,” *Opt. Lett.*, vol. 45, no. 1, pp. 5–8, Dec. 2019, doi: 10.1364/ol.45.000005.

[27] J. N. Kutz, B. C. Collings, K. Bergman, and W. H. Knox, “Stabilized pulse spacing in soliton lasers due to gain depletion and recovery,” *IEEE J. Quantum Electron.*, vol. 34, no. 9, pp. 1749–1757, Sep. 1998, doi: 10.1109/3.709592.

[28] D. A. Korobko, O. G. Okhotnikov, and I. O. Zolotovskii, “Long-range soliton interactions through gain-absorption depletion and recovery,” *Opt. Lett.*, vol. 40, no. 12, pp. 2862–2865, Jun. 2015, doi: 10.1364/ol.40.002862.

[29] R. Weill, A. Bekker, V. Smulakovsky, B. Fischer, and O. Gat, “Noise-mediated Casimir-like pulse interaction mechanism in lasers,” *Optica*, vol. 3, no. 2, pp. 189–192, Feb. 2016, doi: 10.1364/optica.3.000189.

[30] A. Zaviyalov, P. Grelu, and F. Lederer, “Impact of slow gain dynamics on soliton molecules in mode-locked fiber lasers,” *Opt. Lett.*, vol. 37, no. 2, pp. 175–177, Jan. 2012, doi: 10.1364/ol.37.000175.

[31] J. K. Jang, M. Erkintalo, S. G. Murdoch, and S. Coen, “Ultraweak long-range interactions of solitons observed over astronomical distances,” *Nature Photon.*, vol. 7, no. 8, pp. 657–663, Jul. 2013, doi: 10.1038/nphoton.2013.157.

[32] A. N. Pilipetskii, E. A. Golovchenko, and C. R. Menyuk, “Acoustic effect in passively mode-locked fiber ring lasers,” *Opt. Lett.*, vol. 20, no. 8, pp. 907–909, Apr. 1995, doi: 10.1364/ol.20.000907.

[33] H. J. Kbashi, S. V. Sergeyev, M. Al-Araimi, A. Rozhin, D. Korobko, and A. Fotiadi, “High-frequency vector harmonic mode locking driven by acoustic resonances,” *Opt. Lett.*, vol. 44, no. 21, pp. 5112–5115, Oct. 2019, doi: 10.1364/ol.44.005112.

[34] W. He, M. Pang, D.-H. Yeh, J. Huang, C. R. Menyuk, and P. S. Russell, “Formation of optical supramolecular structures in a fibre laser by tailoring long-range soliton interactions,” *Nature Commun.*, vol. 10, no. 1, Dec. 2019, Art. no. 5756, doi: 10.1038/s41467-019-13746-6.

[35] V. A. Ribenek, P. A. Itrin, D. A. Korobko, and A. A. Fotiadi, “Double harmonic mode-locking in soliton fiber ring laser acquired through the resonant optoacoustic coupling,” *Appl. Phys. Lett. Photon.*, vol. 9, no. 5, May 2024, Art. no. 056105, doi: 10.1063/5.0195623.

[36] W. H. Loh, V. V. Afanasjev, D. N. Payne, and A. B. Grudinin, “Soliton interaction in the presence of a weak nonsoliton component,” *Opt. Lett.*, vol. 19, no. 10, pp. 698–700, May 1994, doi: 10.1364/ol.19.000698.

[37] V. A. Ribenek, D. A. Korobko, A. A. Fotiadi, and J. R. Taylor, “Supermode noise mitigation and repetition rate control in a harmonic mode-locked fiber laser implemented through the pulse train interaction with co-lased CW radiation,” *Opt. Lett.*, vol. 47, no. 19, pp. 5236–5239, Sep. 2022, doi: 10.1364/ol.472780.

[38] D. A. Korobko, V. A. Ribenek, D. A. Stoliarov, P. Mégret, and A. A. Fotiadi, “Resonantly induced mitigation of supermode noise in a harmonically mode-locked fiber laser: Revealing the underlying mechanisms,” *Opt. Exp.*, vol. 30, no. 10, pp. 17243–17258, May 2022, doi: 10.1364/oe.457023.

[39] D. Y. Tang, B. Zhao, L. M. Zhao, and H. Y. Tam, “Soliton interaction in a fiber ring laser,” *Phys. Rev. E*, vol. 72, no. 1, Jul. 2005, Art. no. 016616, doi: 10.1103/physreve.72.016616.

[40] D.-H. Yeh, W. He, M. Pang, X. Jiang, G. Wong, and P. S. Russell, “Pulse-repetition-rate tuning of a harmonically mode-locked fiber laser using a tapered photonic crystal fiber,” *Opt. Lett.*, vol. 44, no. 7, pp. 1580–1583, Mar. 2019, doi: 10.1364/ol.44.001580.

[41] S. M. J. Kelly, “Characteristic sideband instability of periodically amplified average soliton,” *Electron. Lett.*, vol. 28, no. 8, p. 806, 1992, doi: 10.1049/el:19920508.

[42] M. L. Dennis and I. N. Duling, “Experimental study of sideband generation in femtosecond fiber lasers,” *IEEE J. Quantum Electron.*, vol. 30, no. 6, pp. 1469–1477, Jun. 1994, doi: 10.1109/3.299472.

[43] C.-J. Chen, P. K. A. Wai, and C. R. Menyuk, “Soliton fiber ring laser,” *Opt. Lett.*, vol. 17, no. 6, pp. 417–419, Mar. 1992, doi: 10.1364/ol.17.000417.

[44] R. V. Gumenyuk, D. A. Korobko, and I. O. Zolotovskii, “Stabilization of passive harmonic mode locking in a fiber ring laser,” *Opt. Lett.*, vol. 45, no. 1, pp. 184–187, Dec. 2019, doi: 10.1364/ol.45.000184.

[45] D. A. Korobko, V. A. Ribenek, P. A. Itrin, D. A. Stoliarov, and A. A. Fotiadi, “Polarization maintaining harmonically mode-locked fiber laser with suppressed supermode noise due to continuous wave injection,” *Opt. Laser Technol.*, vol. 162, Jul. 2023, Art. no. 109284, doi: 10.1016/j.optlastec.2023.109284.

[46] Y. Du, X. Shu, H. Cao, and P. Cheng, “Dynamics of dispersive wave and regimes of different kinds of sideband generation in mode-locked soliton fiber lasers,” *IEEE J. Sel. Topics Quantum Electron.*, vol. 24, no. 3, May/Jun. 2018, Art. no. 1101408, doi: 10.1109/jstqe.2017.2777531.

[47] D. Han and Y. Liao, “Observations of three types of sidebands in a passively mode-locked soliton fiber laser,” *Laser Phys.*, vol. 22, no. 12, pp. 1837–1841, Nov. 2012, doi: 10.1134/s1054660x12120092.

[48] H. Haris et al., “Generation of Kelly and dip type sidebands soliton employing topological insulator (Bi2Te3) as saturable absorber,” *Infrared Phys. Technol.*, vol. 123, Jun. 2022, Art. no. 104154, doi: 10.1016/j.infrared.2022.104154.

[49] H. Haris et al., “Single and bunch soliton generation in optical fiber lasers using bismuth selenide topological insulator saturable absorber,” *Nanomaterials*, vol. 13, no. 9, May 2023, Art. no. 1538, doi: 10.3390/nano13091538.

[50] V. Voropaev et al., “Generation of multi-solitons and noise-like pulses in a high-powered thulium-doped all-fiber ring oscillator,” *Sci. Rep.*, vol. 9, no. 1, Dec. 2019, Art. no. 18369, doi: 10.1038/s41598-019-54563-7.

[51] Y. Song et al., “Period-Doubling and quadrupling bifurcation of vector soliton bunches in a graphene mode locked fiber laser,” *IEEE Photon. J.*, vol. 9, no. 5, Oct. 2017, Art. no. 4502308, doi: 10.1109/jphot.2017.2734163.